Precipitation of highly energetic protons by helium branch electromagnetic ion cyclotron triggered emissions

Shoji, Masafumi; Omura, Yoshiharu

JOURNAL OF GEOPHYSICAL RESEARCH, VOL. 117, A12210, doi:10.1029/2012JA017933, 2012

Precipitation of highly energetic protons by helium branch electromagnetic ion cyclotron triggered emissions

Masafumi Shoji[1,2] and Yoshiharu Omura[2]

Received 10 May 2012; revised 15 October 2012; accepted 16 October 2012; published 8 December 2012.

[1] In the equatorial region of the Earth's inner magnetosphere, the electromagnetic ion cyclotron (EMIC) triggered emissions are generated through interaction with energetic protons. We investigate the generation process of the EMIC triggered emissions in the He^+ branch and associated precipitation of the energetic protons using a one-dimensional hybrid simulation with a cylindrical parabolic magnetic geometry. The simulation results show a good agreement with the nonlinear wave growth theory. As the electron density becomes higher as in the plasmasphere or the plasmaplume, the wave amplitude thresholds for both H^+ and He^+ band triggered emissions become lower and their nonlinear growth rates become higher. The higher hot proton density also makes the thresholds lower. While the H^+ branch triggered emissions interact with a few keV protons, the He^+ branch triggered emissions interact with more energetic protons of a few hundred keV with a larger nonlinear growth rate.

Citation: Shoji, M., and Y. Omura (2012), Precipitation of highly energetic protons by helium branch electromagnetic ion cyclotron triggered emissions, *J. Geophys. Res.*, *117*, A12210, doi:10.1029/2012JA017933.

1. Introduction

[2] Electromagnetic ion cyclotron (EMIC) wave emissions with rising frequencies in the ULF (Ultra Low Frequency) range, so-called EMIC triggered emissions, have been observed by Cluster satellites in the Earth's plasmasphere [*Pickett et al.*, 2010; *Omura et al.*, 2010]. They are generated by small amplitude triggering EMIC waves and anisotropic energetic protons. The triggering EMIC waves are also known as "Pc1 pulsations" observed on the ground [e.g., *Troitskaya*, 1961; *Tepley*, 1961] and in space [e.g., *Roux et al.*, 1982; *Anderson et al.*, 1992a, 1992b; *Engebretson et al.*, 2007]. The energetic protons come into the plasmasphere due to the particle injections during magnetic disturbances such as magnetic storms and substorms [e.g., *Ejiri*, 1978]. These energetic protons constitute the ring currents in the inner magnetosphere [e.g., *Ebihara et al.*, 2002; *Ebihara and Fok*, 2004].

[3] The generation mechanism of EMIC triggered emissions has been studied by the nonlinear theory [*Omura et al.*, 2010] and by hybrid code simulations [*Shoji and Omura*, 2011; *Shoji et al.*, 2011]. Since there are multiple species of ions in the Earth's inner magnetosphere, the dispersion relation of EMIC waves are separated into branches corresponding to the ion populations [e.g., *Stix*, 1992]. In the previous hybrid simulation studies [*Shoji and Omura*, 2011; *Shoji et al.*, 2011], in which protons, heliums, and oxygens are assumed, EMIC triggered emissions in the H^+ branch have been successfully reproduced in a cylindrical magnetic flux model corresponding to the equatorial region of the inner magnetosphere. These real scale simulation results show a good agreement with the observations [*Pickett et al.*, 2010] and the nonlinear growth theory [*Omura et al.*, 2010]. Moreover, *Shoji et al.* [2011] have shown that the multiple EMIC triggered emissions in the H^+ branch induce EMIC waves in the He^+ branch. Simulation results show that pitch angle scattering of a substantial number of energetic protons in the equatorial region results in proton auroras [e.g., *Montbriand*, 1971; *Fukunishi*, 1975] in the polar region.

[4] In the previous papers [e.g., *Pickett et al.*, 2010], the triggered emissions in the H^+ branch have been investigated. EMIC waves in the lower branches also play an important role in the inner magnetosphere. *Summers and Thorne* [2003] and *Summers et al.* [2007] have analyzed the resonant quasi-linear scattering of energetic electrons by EMIC waves in the H^+ and He^+ branches. Although the observations of the EMIC triggered emissions in other branches have not been reported yet, the nonlinear theory predicts existence of the EMIC triggered emissions with rising frequencies in the He^+ and O^+ branches [*Omura et al.*, 2010]. The triggered emissions in the different branches can scatter energetic protons in different energy ranges, since the emissions have different resonance velocities. Especially, triggered emissions in the lower branches will strongly contribute to proton auroras in higher energy ranges.

[5] The main objective of the present study is to reproduce EMIC triggered emissions in the He^+ branch by computer simulations to estimate the impact of the He^+ band triggered emissions on pitch angle scattering in the equatorial region.

[1]Institute of Space and Astronautical Science, Japan Aerospace Exploration Agency, Sagamihara, Japan.
[2]Research Institute for Sustainable Humanosphere, Kyoto University, Uji, Japan.

Corresponding author: M. Shoji, Institute of Space and Astronautical Science, Japan Aerospace Exploration Agency, 3-1-1 Yoshinodai, Chuo-ku, Sagamihara, Kanagawa 252-5210, Japan. (shoji@stp.isas.jaxa.jp)

0148-0227/12/2012JA017933

Table 1. Parameters of the Simulation Space, Time, Static Magnetic Field, Electron Fluid, and Triggering Waves

Parameters	Normalized Value	Real Value
Number of grids N_x	4096	
Number of grids of damping region N_{rx}	1536	
Grid spacing Δx	0.1 V_A/Ω_H	1.9 km
Time step Δt	0.004/Ω_H	1.72×10^{-4} s
Proton cyclotron frequency at the equator $f_H = \Omega_H/(2\pi)$	1/(2π)	3.7 Hz
Electron cyclotron frequency at the equator $f_e = \Omega_e/(2\pi)$	1836 f_H	6.8 kHz
Proton plasma frequency at the equator $f_{pH} = \Omega_{pH}/(2\pi)$	95.5 f_H	353.4 Hz
Electron plasma frequency at the equator f_{pe}	339.8 f_e	120.1 kHz
Ambient magnetic field at the equator B_{0eq}	1	243 nT
Alfven velocity at the equator V_A	1.0	443 km/s
Frequency of triggering wave f_w	0.15 f_H	0.56 Hz
Wave number of triggering wave k_w	0.135 Ω_H/V_A	1.1×10^{-3}/km
Amplitude of triggering wave B_{w0}	$2.1 \times 10^{-4} B_{0eq}$	0.05 nT

We perform a real scale hybrid simulation with a parabolic dipole magnetic geometry. A simulation of EMIC triggered emissions in the He^+ branch is presented in section 2. We study nonlinear interaction between He^+ branch triggered emissions and highly energetic protons and analyze time evolution of the velocity distribution functions.

[6] In section 3, we compare the simulation results with the nonlinear wave growth theory [*Omura et al.*, 2010] for the He^+ branch triggered emissions. Possibility of generation of the He^+ and H^+ branch triggered emissions is discussed by calculating the theoretical thresholds and nonlinear growth rates. We also estimate kinetic energies of hot protons interacting with the triggered emissions in the different (H^+ and He^+) branches. We summarize the present study in section 4.

2. Hybrid Simulation for the He^+ Branch Triggered Emission

2.1. Simulation Model and Parameters

[7] We have developed a one-dimensional (1D) hybrid code [*Shoji et al.*, 2009]. The code has been expanded to a cylindrical magnetic flux model [*Shoji and Omura*, 2011; *Shoji et al.*, 2011] described as $B_{0x}(x) = B_{0eq}(1 + ax^2)$, where B_{0eq} is the value at the equator, $a = 4.5/(LR_E)^2$, $L = 4.3$ and the Earth's radius R_E = 6387 km. To satisfy the condition $\nabla \cdot \mathrm{B} = 0$, the radial component of the ambient magnetic field is assumed as $B_{0r} = -0.5 r_{Li}\, \partial B_{0x}/\partial x$, where $r_{Li} = v_\perp/\Omega_{ci}$ is the Larmor radius of an ion, and Ω_{ci} is the local cyclotron frequency of ions of species i. While the field equations are solved as the 1D system taken along the x axis, the background magnetic field has a cylindrical geometry around the x axis, and ions are assumed to gyrate around the magnetic field with finite cyclotron radii. The triggering waves are excited at the equator by an external current source. The parallel components of the electric field and current density are not solved, since we only have purely transverse waves propagating along the magnetic field line in the present simulation. An open boundary condition is assumed for the x direction with damping layers attached at both ends of the physical region. The transverse wave magnetic fields are damped as $B_{damp}(x) = r(x)B(x)$ at each time step, where $r(x)$ is a masking function [*Umeda et al.*, 2001; *Shoji et al.*, 2012]. Assuming the mirror motion of the particles in the dipole magnetic field, particles going out of the simulation space are reflected at each boundary. To obtain forward and backward coherent monochromatic L-mode EMIC waves without R-mode noise, we use a left-handed polarized current source. The current source is modeled by five grid points around the equatorial region. We oscillate the phase of the middle grid with the frequency of the triggering waves, and oscillate phases of the adjacent two grids on both sides with phase differences corresponding to the wave numbers of the forward and backward traveling triggering waves. To suppress an initial response of the magnetic field to the source current, we increase the magnitude of the current gradually in time.

[8] We use realistic values in the observations at the equator close to the plasmapause ($L \sim 4$) [*Pickett et al.*, 2010; *Omura et al.*, 2010] as initial parameters and shown in Table 1. The frequency of the triggering wave excited by the left-handed polarized current source at the equator is defined near the cut-off frequency of the He^+ branch. The wave numbers of the triggering wave are calculated from the linear EMIC dispersion relation. Cold plasma components of H^+, He^+ and O^+ ions are assumed, and their thermal distributions are neglected. The energetic protons are also assumed as resonant components with the EMIC waves. The thermal velocities for parallel and perpendicular directions, ion density ratios to the electron density, charge-to-mass ratios, and numbers of superparticles of these ions are listed in Table 2. Their densities are assumed so that the wave dispersion relation gives the cut-off frequencies observed around the equatorial region at $L \sim 4$ [*Omura et al.*, 2010]. Energetic protons form a loss cone distribution function [*Shoji and Omura*, 2011].

[9] The energetic protons are distributed uniformly with a subtracted bi-Maxwell distribution function in the whole space. Since the given distribution function is not stable in the nonuniform magnetic field, we solve motion of the

Table 2. Simulation Parameters of the Ion Species

Ion Species	$V_{th\|\|}/c$	$V_{th\perp}/c$	n_i/n_e	$q/m/(e/m_H)$	N_p/cell
H^+	0	0	0.8019	1.0	256
He^+	0	0	0.0950	1/4	256
O^+	0	0	0.0950	1/16	256
Hot H^+	0.008	0.01068	0.0081	1.0	16,384

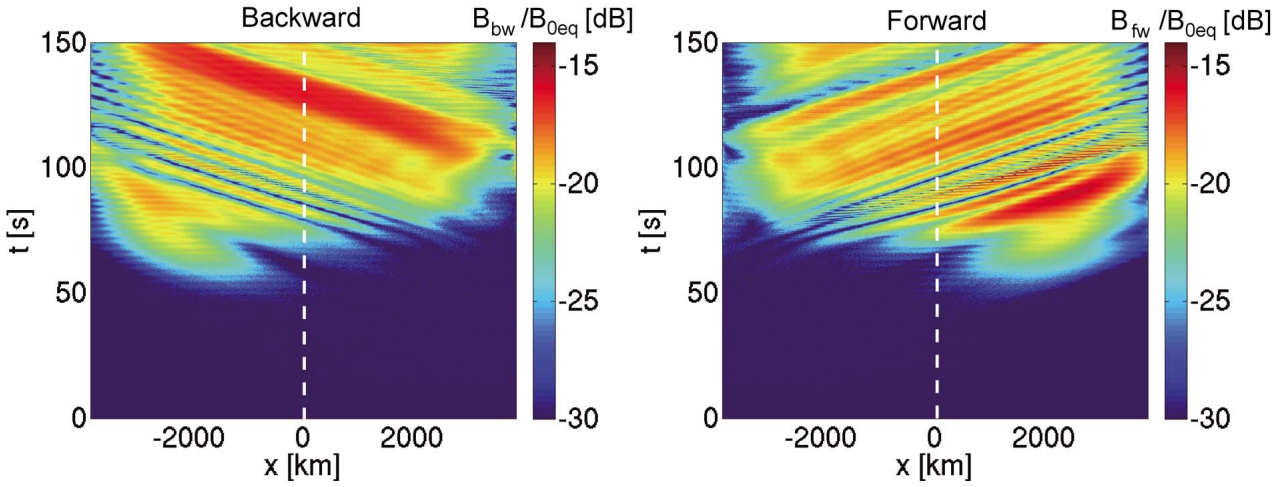

Figure 1. Spatial and temporal evolution of the wave amplitudes of the backward and forward propagating EMIC waves.

particles in the absence of the electromagnetic fluctuations until the spatial distribution becomes stable in time. We then prepare another set of protons with the same x, $v_{\parallel}$ and $v_{\perp}$ and opposite gyrophases to suppress initial electromagnetic thermal fluctuations in the distribution function (so-called quiet start [*Birdsall and Langdon*, 1985]). We use the obtained distribution function as the initial condition.

2.2. Generation of the He^+ Branch Triggered Emission

[10] Figure 1 shows spatial and temporal evolutions of the amplitudes of the backward and forward propagating waves. The particles moving in the opposite directions of the wave propagation are phase organized by the triggering waves which are generated at the equator (shown by the dashed white line). These particles are released at the equator generating seeds of the triggered emissions.

[11] Figure 2a shows the dynamic spectra of the forward propagating waves separated from the magnetic field data by the method used in *Shoji and Omura* [2011]. The wave with rising frequency below the He^+ cyclotron frequency (dashed white line) appears after $t \sim 85$ s. The wave amplitude of the forward propagating wave in logarithmic scale is shown in Figure 2b. The theoretical threshold for EMIC triggered emissions given by (62) of *Omura et al.* [2010] becomes $B_w = 0.48$ nT with the present parameters. We show the threshold by the dashed blue line in Figure 2b. Although the initial wave amplitude of the triggering wave (0.05 nT) does not reach the theoretical threshold, the amplitude becomes larger through the linear growth of the EMIC waves in $0 < t < 85$ s. The dashed red line shows the linear growth rate calculated from the kinetic dispersion relation [*Stix*, 1992]. Since some EMIC modes grow at the same time, the amplitude is modulated at this stage. After the wave amplitude exceeds the threshold, the nonlinear wave growth starts. In $t > 85$ s, the wave frequency starts rising and the nonlinear growth of the triggered wave becomes faster than the linear growth (shown by the dashed red line). The EMIC triggered emission saturates at $B_w = 3.5$ nT (dash-dotted blue line) around $t \sim 105$ s and rising of the frequency stops at 0.8 Hz around $t \sim 130$ s. The frequency varies from 0.56 Hz to

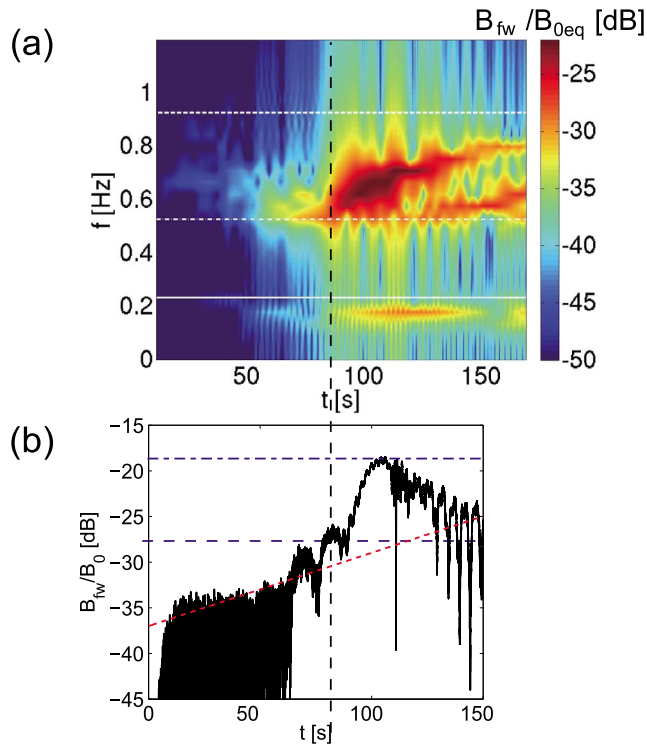

Figure 2. (a) Dynamic spectra of the magnetic field of forward propagating waves. The solid, dash-dotted, and dashed white lines show the cyclotron frequency of O^+, the theoretical frequency of the triggered waves, and the cyclotron frequency of He^+, respectively. (b) Time evolution of the wave amplitude at the equator in log scale. The dashed red line shows the linear growth rate of the EMIC wave. The dashed and dash-dotted blue lines show the theoretical threshold $B_w = 0.48$ nT and the saturation level $B_{sat} = 3.5$ nT of the EMIC triggered emission, respectively. The dashed black line shows the time when the nonlinear wave growth starts ($t \sim 85$ s).

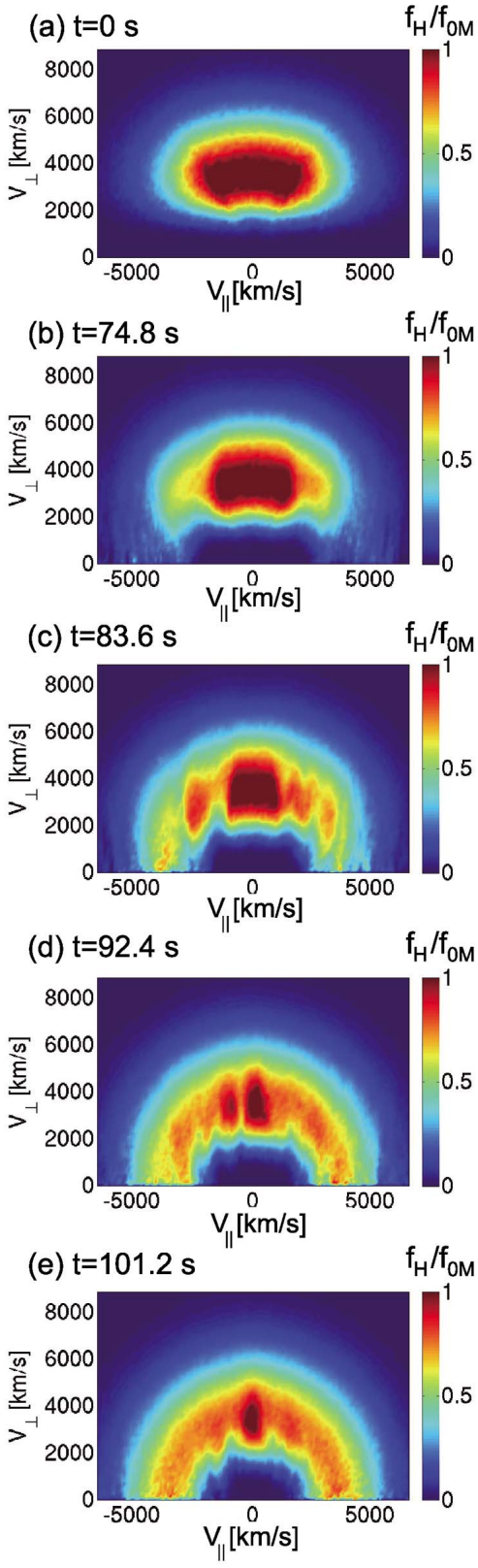

Figure 3. Velocity distribution functions $f_H(v_\parallel, v_\perp)$ of energetic protons at (a) t = 0 s, (b) t = 74.8 s, (c) t = 83.6 s, (d) t = 92.4 s, and (e) t = 101.2 s normalized by the maximum value of the initial velocity distribution function f_{0M}.

0.8 Hz in 45 s. The O^+ band EMIC emission and another triggered emission are also generated because of the pitch angle scattering mechanism discussed in *Shoji et al.* [2011].

2.3. Time Evolution of the Velocity Distribution Function

[12] The time history of the velocity distribution function of the energetic protons at the magnetic equator is shown in Figure 3. In Figure 3a, we show the initial velocity distribution function. In Figure 3b, the energetic protons around the resonance velocity of the triggering waves $V_R = (\omega - \Omega_H)/k = 2$, 900 km/s, are scattered. The proton holes around the resonance velocity of the triggered emissions appear in Figure 3c. Inward motion of the proton holes is also tracked in the velocity distribution function through Figures 3c, 3d and 3e. Because of existence of the huge proton holes, the core part of the distribution function is scattered as shown in Figure 3d. Finally, the distribution function is significantly modified in Figure 3e.

[13] The pitch angles of the energetic protons are scattered by the He^+ band EMIC triggered emissions and some of the protons go into the loss cone (4.8 degrees). The amount of the protons going into the loss cone is estimated by the same method as in *Shoji and Omura* [2011]. At $t \sim 150$ s, the triggered emissions in the He^+ branch scatter 6.4% of the hot proton population around the equatorial region (-210 km $< x <$ 210 km) into the loss cone. The mean energy of the precipitated protons is 90 keV. On the other hand, the H^+ branch EMIC triggered emissions scatter the hot protons with kinetic energy ~4.5 keV into the loss cone [*Shoji and Omura*, 2011]. Because the resonance velocity of the He^+ band triggered wave is larger than that of the H^+ band triggered waves for the EMIC triggered emissions (V_R = 970 km/s) [*Shoji and Omura*, 2011], the energy range of the scattered protons becomes larger.

3. Theoretical Models of Nonlinear Wave Growth

3.1. Comparison With the Simulation Result

[14] *Omura et al.* [2010] have performed a theoretical analysis for the H^+ branch triggered emissions. Theoretical frequency sweep rates with different initial wave amplitudes and nonlinear growth rates for the He^+ branch triggered emissions are also obtained by solving the equations (63) and (64) of *Omura et al.* [2010]. The value of Q, which was also introduced by *Omura et al.* [2010], is a factor representing a depth of a proton hole in the distribution function given by

$$g(\zeta, v_\parallel) = g_0(v_\parallel) - Q g_{tr}(v_\parallel, \zeta), \quad (1)$$

where ζ is the angle between $v_\perp$ and the wave magnetic field. The functions $g_0(v_\parallel)$ and $g_{tr}(v_\parallel, \zeta)$ are an unperturbed velocity distribution function of protons, and a part of g_0 that is trapped by the wave, respectively. We assume the saturation at B_w = 3.5 nT, which is obtained from the hybrid simulation result shown in Figure 2b. In the nonlinear growth phase, we assume Q = 0.5. To reproduce the dissipation of the triggered emission after the saturation, we assume that Q changes from 0.5 to 0.1 after the amplitude reaches 3.5 nT.

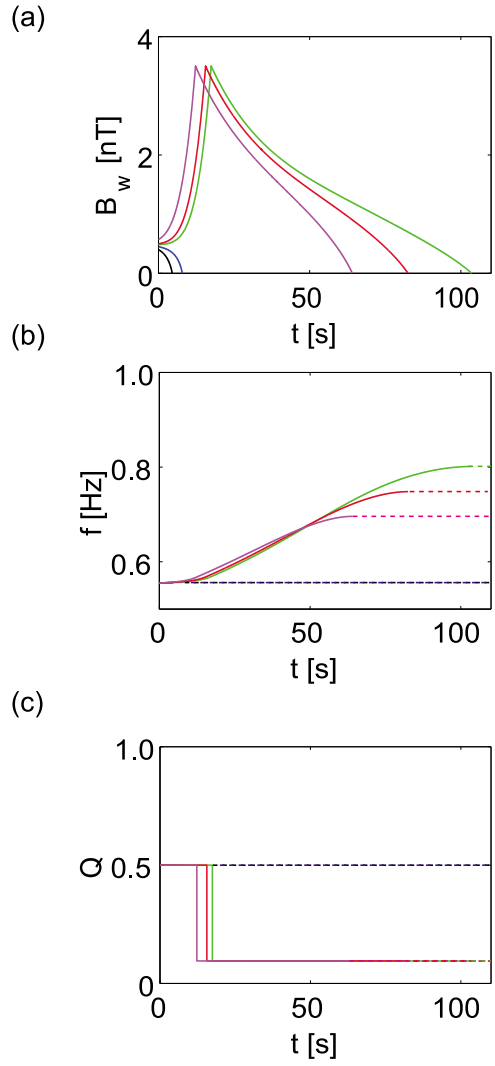

Figure 4. Theoretical models of (a) the wave amplitude, (b) the frequency sweep rate of the EMIC triggered emissions below the He^+ cyclotron frequency, and (c) depth of proton holes Q at the equator. The magenta, green, black, blue, and red lines show the results with the amplitudes of the triggering waves 0.4 nT, 0.45 nT, 0.49 nT, 0.5 nT, and 0.57 nT, respectively.

[15] Time evolutions of wave amplitudes and the frequency sweep rates of EMIC triggered emissions at the equator for different initial amplitudes are shown in Figures 4a and 4b, respectively. The time variation of Q is also shown in Figure 4c. In cases that the initial amplitudes are assumed lower than the theoretical threshold given by (54) of *Omura et al.* [2010] ($B_w < 0.48$ nT), the triggered emissions do not take place as shown in Figure 4, because the linear wave growth is not included in the nonlinear growth theory. In cases with initial amplitudes larger than the threshold, we can find the nonlinear wave growth in Figure 4a, and the rising frequency in Figure 4b (shown by green, red, and magenta lines). The nonlinear growth stops around 11 s, 16 s, and 19 s for red, blue, and black cases, respectively. Comparing the theoretical result (green line case obtained with an initial wave amplitude of 0.49 nT) with the simulation result, we find that the durations of the nonlinear wave growth and of the dissipation agree with the simulation. The frequency sweep rate of the He^+ branch triggered emission from 0.56 Hz to 0.8 Hz also shows a good agreement.

3.2. Thresholds and Nonlinear Growth Rates of H^+ and He^+ Band Triggered Emissions

[16] The nonlinear wave growth starts when the amplitude reaches the theoretical threshold given by *Omura et al.* [2010]. To estimate the possibility of the generation of the triggered emissions in the different regions and conditions, we plot the thresholds B_{th} of the H^+ and He^+ branch triggered emissions as functions of the electron density and the wave frequency with different energetic proton densities in Figure 5. The white circles indicate the input parameters used in the present He^+ branch simulation and the previous H^+ branch simulation [*Shoji and Omura*, 2011], respectively. In Figures 5a and 5c, we show the thresholds with the parameters (hot proton density) that we used in the present simulation. In Figures 5b and 5d, on the other hand, we plot the thresholds for higher hot proton density (4.05%), that is used in *Shoji and Omura* [2011]. Here, we note that the frequency range of Figures 5a and 5b is different from that of Figures 5c and 5d. The range of the colorbar of these panels are taken as $0 < B_{th}/B_0 < 0.1$ for possible triggering wave amplitudes. As a reference, we plot dashed white lines (the electron density of 50/cc) to indicate the regions outside and inside the possible plasmapause based on the observation [*Pickett et al.*, 2010]. In the high electron density region corresponding to the plasmasphere, both He^+ and H^+ band triggered emissions have thresholds low enough to be generated in any cases shown in Figure 5. On the other hand, in the low electron density region, the thresholds become higher as shown in Figures 5a and 5c, as we can obviously find in (62) of *Omura et al.* [2010]. In Figures 5b and 5d, because of the denser population of the energetic protons, the thresholds of both triggered emissions keep low values even outside the plasmapause.

[17] The nonlinear growth rate of the EMIC triggered emissions is given by (54) of *Omura et al.* [2010]. We plot the nonlinear growth rates for both H^+ and He^+ branch triggered emissions as functions of the frequency and the electron density in Figures 6a and 6b. Here, we note that the frequency range of Figures 6a and 6b is different from that of Figures 6c and 6d. Because the nonlinear growth rate is proportional to the energetic proton density ($\propto \omega_{ph}^2$) as shown in (54) of *Omura et al.* [2010], we only show a case with the energetic proton density $n_h/n_e = 4.05\%$ corresponding to Figures 5b and 5d. The He^+ and H^+ branch triggered emissions have their maximum nonlinear growth rates at $\omega/\Omega_H \sim 0.18$ and $\omega/\Omega_H \sim 0.59$, respectively, with the highest cold electron density. Comparing Figure 6a with Figure 6c, we find that the He^+ branch triggered emissions have larger growth rate than the H^+ branch triggered emissions. However, the nonlinear growth rates do not control the frequency sweep rates of the triggered emissions, which depend on (saturated amplitude) × (frequency) of the emissions [*Omura et al.*, 2010].

[18] We also show the kinetic energies of the resonant particles of the He^+ and H^+ branch triggered emissions for

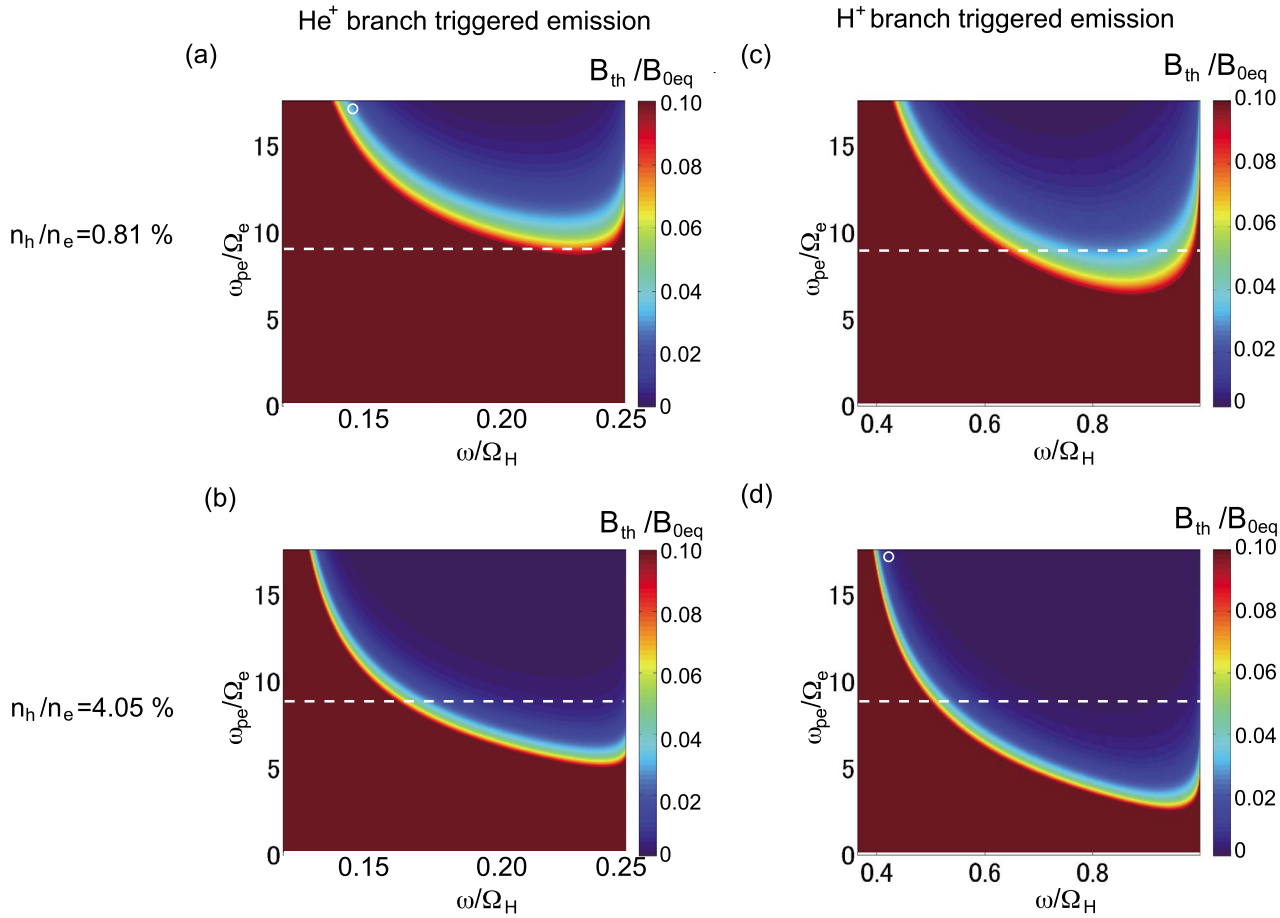

Figure 5. Theoretical thresholds of nonlinear wave growth as functions of frequency f and electron density n_e for He^+ branch triggered emissions with densities of energetic protons (a) n_h/n_e = 0.81% and (b) n_h/n_e = 4.05%, and those for H^+ branch triggered emissions with densities of energetic protons (c) n_h/n_e = 0.81% and (d) n_h/n_e = 4.05%. The ambient magnetic field, the proton cyclotron frequency, and the electron cyclotron frequency at the equator are B_{0eq} = 243 nT, Ω_H = 23.2 rad/s, and Ω_e = 4.27 × 10^4 rad/s, respectively. The dashed white lines indicate an electron density 50/cc corresponding to the possible plasmapause. The white circles in Figures 5a and 5d indicate the input parameters used in the present He^+ branch simulation and the previous H^+ branch simulation [*Shoji and Omura*, 2011], respectively.

different electron densities in Figures 6b and 6d, respectively, assuming that the resonant particles have a pitch angle $\theta_c = 40°$. For high electron densities, the kinetic energy of a proton K_R resonating with the He^+ branch triggered emission reaches around a few hundred keV, while that of protons interacting with the H^+ branch emission is a few keV. As the density of the electrons becomes smaller, the kinetic energy of the resonant particles becomes larger. As the frequencies of the triggered emissions become smaller, these kinetic energies become larger as shown in Figures 6b and 6d.

4. Summary

[19] We performed the simulation for the EMIC triggered emissions in the He^+ branch, which have been found in spacecraft observations [e.g., *Grison et al.*, 2011]. The energies of protons scattered by the He^+ band EMIC triggered emissions are much larger than those of protons scattered by the H^+ branch triggered emissions. As reported in *Shoji et al.* [2011], multiple triggered emissions induce another type of EMIC wave in the lower frequency branch. In the present simulation, the O^+ branch EMIC wave is generated as shown in Figure 2a because of the strong modification of the velocity distribution function of the energetic protons.

[20] The strong modification of the velocity distribution function results from the inward motion of the proton holes, as described by *Shoji and Omura* [2011] in the H^+ branch triggered emission case. Some parts of the proton aurora in the different energy ranges can be caused by the triggered emissions in the different branches. Both H^+ and He^+ triggered emissions have thresholds low enough to cause the nonlinear wave growth in the case of the high electron densities such as inside the plasmasphere or the plasmaplume. The thresholds also become lower as the hot proton density becomes larger. The emissions also have higher nonlinear growth rates for higher electron densities. For the

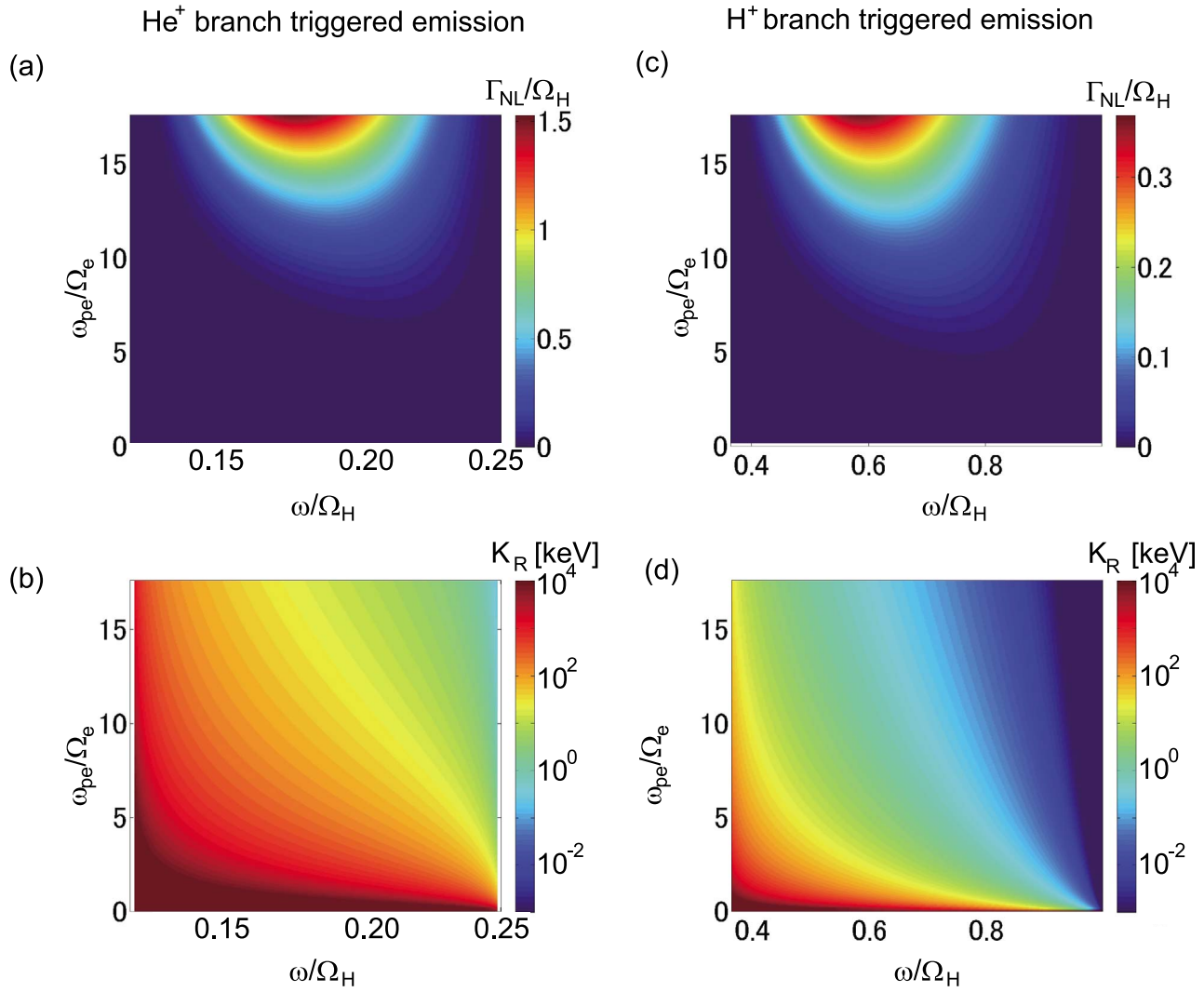

Figure 6. Nonlinear growth rate Γ_{NL} of the EMIC triggered emissions with the wave amplitudes at the theoretical threshold, and kinetic energy of the energetic protons with $v_{\|} = V_R$ as functions of frequency f and electron density n_e for the (a and b) He^+ branch triggered emissions and for the (c and d) H^+ branch triggered emissions. The ambient magnetic field, the proton cyclotron frequency, and the electron cyclotron frequency at the equator are $B_{0eq} = 243$ nT, $\Omega_H = 23.2$ rad/s, and $\Omega_e = 4.27 \times 10^4$ rad/s, respectively.

maximum growth rates of the He^+ and H^+ band triggered emissions, resonant protons have the kinetic energies around a few hundred keV and a few keV, respectively.

[21] Since we used the 1D model, generation and propagation of waves in the oblique directions are not solved. In a 2D model with a nonuniform magnetic field, refraction of EMIC waves is also important. Expansion of the present model to the 2D nonuniform system is left as a future study.

[22] **Acknowledgments.** Computation in the present study was performed with the KDK system of Research Institute for Sustainable Humanosphere and Academic Center for Computing and Media Studies at Kyoto University as a collaborative research project. The present study was supported in part by a Grant-in-Aid for Research Fellows from the Japan Society for the Promotion of Science, and Grant-in-Aid 23340147 of the Ministry of Culture, Sports, Science, and Technology in Japan.

[23] Robert Lysak thanks the reviewers for their assistance in evaluating this paper.

References

Anderson, B. J., R. E. Erlandson, and L. J. Zanetti (1992a), A statistical study of Pc 1–2 magnetic pulsations in the equatorial magnetosphere: 1. Equatorial occurrence distributions, *J. Geophys. Res.*, *97*, 3075, doi:10.1029/91JA02706.

Anderson, B. J., R. E. Erlandson, and L. J. Zanetti (1992b), A statistical study of Pc 1–2 magnetic pulsations in the equatorial magnetosphere: 2. Wave properties, *J. Geophys. Res.*, *97*, 3089, doi:10.1029/91JA02697.

Birdsall, C. K., and A. B. Langdon (1985), *Plasma Physics via Computer Simulation*, McGraw-Hill, New York.

Ebihara, Y., and M.-C. Fok (2004), Postmidnight storm-time enhancement of tens-of-keV proton flux, *J. Geophys. Res.*, *109*, A12209, doi:10.1029/2004JA010523.

Ebihara, Y., M. Ejiri, H. Nilsson, I. Sandahl, A. Milillo, M. Grande, J. F. Fennell, and J. L. Roeder (2002), Statistical distribution of the storm-time proton ring current: POLAR measurements, *Geophys. Res. Lett.*, *29*(20), 1969, doi:10.1029/2002GL015430.

Ejiri, M. (1978), Trajectory traces of charged particles in the magnetosphere, *J. Geophys. Res.*, *83*(A10), 4798, doi:10.1029/JA083iA10p04798.

Engebretson, M. J., et al. (2007), Cluster observations of Pc 1]2 waves and associated ion distributions during the October and November 2003 magnetic storms, *Planet. Space Sci.*, *55*, 829.

Fukunishi, H. (1975), Dynamic relationship between proton and electron auroral substorms, *J. Geophys. Res.*, *80*, 553, doi:10.1029/JA080i004p00553.

Grison, B., et al. (2011), Propagation of EMIC triggered emissions toward the magnetic equatorial plane, Abstract SM13B-2068 presented at 2011 Fall Meeting, AGU, San Francisco, Calif., 5–9 Dec.

Montbriand, L. E. (1971), The proton aurora and auroral substorm, in *The Radiating Atmosphere*, edited by B. M. McCormac, p. 366, D. Reidel, Dordrecht, Netherlands.

Omura, Y., J. Pickett, B. Grison, O. Santolik, I. Dandouras, M. Engebretson, P. M. E. Decreau, and A. Masson (2010), Theory and observation of electromagnetic ion cyclotron triggered emissions in the magnetosphere, *J. Geophys. Res.*, *115*, A07234, doi:10.1029/2010JA015300.

Pickett, J. S., et al. (2010), Cluster observations of EMIC triggered emissions in association with Pc1 waves near Earth's plasmapause, *Geophys. Res. Lett.*, *37*, L09104, doi:10.1029/2010GL042648.

Roux, A., S. Perraut, J. Rauch, C. de Villedary, G. Kremser, A. Korth, and D. Young (1982), Wave-particle interactions near Ω_{He} observed on board GEOS 1 and 2: 2. Generation of ion cyclotron waves and heating of He + ions, *J. Geophys. Res.*, *87*, 8174, doi:10.1029/JA087iA10p08174.

Shoji, M., and Y. Omura (2011), Simulation of electromagnetic ion cyclotron triggered emissions in the Earth's inner magnetosphere, *J. Geophys. Res.*, *116*, A05212, doi:10.1029/2010JA016351.

Shoji, M., Y. Omura, B. T. Tsurutani, O. P. Verkhoglyadova, and B. Lembege (2009), Mirror instability and L-mode electromagnetic ion cyclotron instability: Competition in the Earth's magnetosheath, *J. Geophys. Res.*, *114*, A10203, doi:10.1029/2008JA014038.

Shoji, M., Y. Omura, B. Grison, J. Pickett, and I. Dandouras (2011), Electromagnetic ion cyclotron waves in the helium branch induced by multiple electromagnetic ion cyclotron triggered emissions, *Geophys. Res. Lett.*, *38*, L17102, doi:10.1029/2011GL048427.

Shoji, M., Y. Omura, and L.-C. Lee (2012), Multidimensional nonlinear mirror-mode structures in the Earth's magnetosheath, *J. Geophys. Res.*, *117*, A08208, doi:10.1029/2011JA017420.

Stix, T. H. (1992), *Waves in Plasmas*, Am. Inst. of Phys., College Park, Md.

Summers, D., and R. M. Thorne (2003), Relativistic electron pitch-angle scattering by electromagnetic ion cyclotron waves during geomagnetic storms, *J. Geophys. Res.*, *108*(A4), 1143, doi:10.1029/2002JA009489.

Summers, D., B. Ni, and N. P. Meredith (2007), Timescales for radiation belt electron acceleration and loss due to resonant wave-particle interactions: 2. Evaluation for VLF chorus, ELF hiss, and electromagnetic ion cyclotron waves, *J. Geophys. Res.*, *112*, A04207, doi:10.1029/2006JA011993.

Tepley, L. R. (1961), Observations of hydromagnetic emissions, *J. Geophys. Res.*, *66*, 1651, doi:10.1029/JZ066i006p01651.

Troitskaya, V. A. (1961), Pulsation of the Earth's electromagnetic field with periods of 1 to 15 seconds and their connection with phenomena in the high atmosphere, *J. Geophys. Res.*, *66*, 5, doi:10.1029/JZ066i001p00005.

Umeda, T., Y. Omura, and H. Matsumoto (2001), An improved masking method for absorbing boundaries in electromagnetic particle simulations, *Comput. Phys. Commun.*, *137*, 286.